Phase-dependent bistable transitions in a weakly-coupled GaAs/AlAs superlattice

2008 New J. Phys. 10 033019

(http://iopscience.iop.org/1367-2630/10/3/033019)

New Journal of Physics
The open-access journal for physics

Phase-dependent bistable transitions in a weakly-coupled GaAs/AlAs superlattice

H T He[1], Y Q Wang[2], W K Ge[1] and J N Wang[1,3]

[1] Department of Physics, Hong Kong University of Science and Technology, Clear Water Bay, Kowloon, Hong Kong, People's Republic of China
[2] Institute of Solid State Physics, Chinese Academy of Sciences, Hefei, Anhui, People's Republic of China
E-mail: phjwang@ust.hk

New Journal of Physics **10** (2008) 033019 (9pp)
Received 24 January 2008
Published 12 March 2008
Online at http://www.njp.org/
doi:10.1088/1367-2630/10/3/033019

Abstract. The bistability between a stable fixed point (SFP) state and a stable limit cycle (SLC) state is observed at the saddle-node bifurcation of cycles occurring in a weakly-coupled GaAs/AlAs superlattice. Controlled transitions between SLC and SFP are induced by external voltage pulses. Intrinsic phase dependence of the transition from SLC to SFP is clearly demonstrated. Using a discrete drift model the experimental observations can be simulated.

Contents

[3] Author to whom any correspondence should be addressed.

1. Introduction

Vertical transport of semiconductor superlattices (SLs) has been studied extensively in the past few decades. Many interesting transport phenomena have been revealed both experimentally and theoretically in SLs, such as saw-tooth-like I–V characteristics [1]–[4], self-sustained current oscillations (SSCOs) [5]–[8], chaos [9]–[11], U-sequence [12] and coherence resonance [13]. Bistability has also been shown inherent in the vertical transport properties of SLs [3, 4, 6, 14]. It can exist between some stable fixed points (SFPs) [3, 4], or between an SFP and a stable limit cycle (SLC) [6, 14]. Here, the SFP and SLC correspond to static currents and SSCOs at a given dc bias, respectively [15, 16]. The bistability between SFPs arises from the location of domain boundary in different quantum wells at the same dc bias [3, 4]. On the other hand, Kastrup *et al* [6] theoretically predicted the existence of bistability between SFP and SLC in SLs and then Luo *et al* [14] observed this bistability experimentally in an undoped photoexcited GaAs/AlAs SL within a certain range of laser intensities. In both cases SLs were in a parameter region where SSCOs, i.e. SLCs, were observed throughout the first tunneling plateau and the bistable region only appeared near the edge of the plateau. In the present work, bistability between SFP and SLC is observed in a doped GaAs/AlAs SL without photoexcitation and the SL is tuned in another parameter region where dynamic voltage bands (DVBs) and static voltage bands appear alternatively on the first tunneling plateau [17]. A DVB corresponds to a voltage interval in each saw-tooth-like current branch where SSCOs are observed. By sweeping the I–V curve on the plateau both in sweep-up and sweep-down directions, a hysteresis is clearly observed at the right boundary of each DVB, which corresponds to a bistability between SFP and SLC. The bistable region is shown to end via a subcritical Hopf bifurcation at the left side and a saddle-node bifurcation of cycles at the right side. We further investigate the transition between SFP and SLC in this bistable region by using a rectangular voltage pulse as a short perturbation to the SL. It reveals an intrinsic phase dependence in the bistable transition from SLC to SFP. A numerical simulation based on a discrete drift model [18, 19] reproduces all the experimental observations. Our work also indicates that the pulse-induced transition scheme can be a possible way to explore the attracting basins of SLC and SFP in the phase space.

2. Experimental

The GaAs/AlAs SL sample used in this work was grown by molecular beam epitaxy. It consists of 30 periods of 14 nm GaAs well and 4 nm AlAs barrier and is sandwiched between two n^+-GaAs layers. The central 10 nm of each GaAs well is doped with Si ($n = 2 \times 10^{17}\,\mathrm{cm}^{-3}$). The sample is fabricated into $0.2 \times 0.2\,\mathrm{mm}^2$ mesas. The time-averaged I–V curve is measured by an HP 4155A semiconductor analyzer. In order to investigate the phase dependence of the transition from SLC to SFP an experimental set-up shown in figure 1 is utilized. The HP 4155A semiconductor analyzer functions as a dc voltage source. The real time current signal through the SL sample flows into a Stanford SR570 low noise current preamplifier whose input is virtually grounded. The SR570 amplifies and converts the current signal into a voltage signal, which is then simultaneously monitored by an Agilent Infiniium 54830B digital oscilloscope and fed into a home-made comparator (ADC) with adjustable reference level. The output of the comparator, which is a transistor–transistor logic (TTL) signal with the high level at 5 V and low level at 0 V, is connected to the trigger input of an Agilent 33220A function generator. At the rising edge of the TTL signal, the function generator is triggered to output a specific

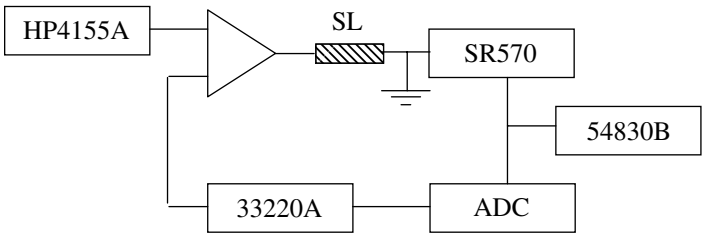

Figure 1. Experimental set-up for the investigation of the phase-dependent transition from SLC to SFP.

rectangular voltage pulse to the SL sample. By tuning the reference level of the comparator a voltage pulse can be generated at a well-defined phase position of the SSCO signal. In the study of the transition from SFP to SLC, the function generator is triggered manually and the comparator is disconnected from the circuit shown in figure 1.

3. Experimental results and discussions

3.1. Bistability and saddle-node bifurcation of cycles

Figure 2(a) shows the measured time-averaged I–V curve on the first tunneling plateau when the sample temperature (T) is fixed at 100.2 K. The I–V curve is measured both in sweep-up (open square) and sweep-down (open triangle) directions. Hysteresis is clearly observed at the right boundary of each temperature-induced DVB [17]. Figure 2(b) shows the enlargement of the second hysteresis which is indicated by a vertical arrow in figure 2(a). The hysteresis behavior indicates the presence of bistability here. On the upper branch of the I–V curve shown in figure 2(b), the current is static, corresponding to an SFP solution in the phase space, while the current on the lower branch is oscillatory, corresponding to an SLC solution. Figure 2(c) shows an SSCO obtained on the lower branch with the dc bias of 473.2 mV. The period of it (τ) is about 280 μs. Thus weakly-coupled semiconductor SLs constitute a class of bistable nonlinear systems between SFP and SLC in the DVB regime. Although the bistability between SFP and SLC has been observed in an undoped photoexcited GaAs/AlAs SL, the bistability only appears near the edge of the first plateau and the upper and lower photocurrent branches in the hysteresis correspond to an SLC and an SFP solution, respectively [14]. But here the bistability is observed in each DVB on the plateau and the upper and lower current branches correspond to an SFP and an SLC solution, respectively.

The observed bistability between an SFP and an SLC at the right boundary of a DVB can be reproduced using the discrete drift model, which has been widely adopted to study the transport properties of weakly-coupled SLs [18, 19]. Since the bistability can also be observed in DVBs on the second tunneling plateau (data not shown), the diffusion component of the total current which is generally considered on the first tunneling plateau has been neglected in the simulation for simplicity. For detailed information about the model and parameters we used in the simulation, please refer to our recent work [20]. Based on the drift velocity curve shown in figure 3(a), a part of the current density (J) versus dc voltage (V_{dc}) curve on the first tunneling plateau is calculated both in sweep-up (open square) and sweep-down (open triangle) directions, as shown in figure 3(b). Similar to figure 2(b), hysteresis behavior is clearly observed at the right boundary of a DVB, with the upper branch corresponding to an SFP solution and the

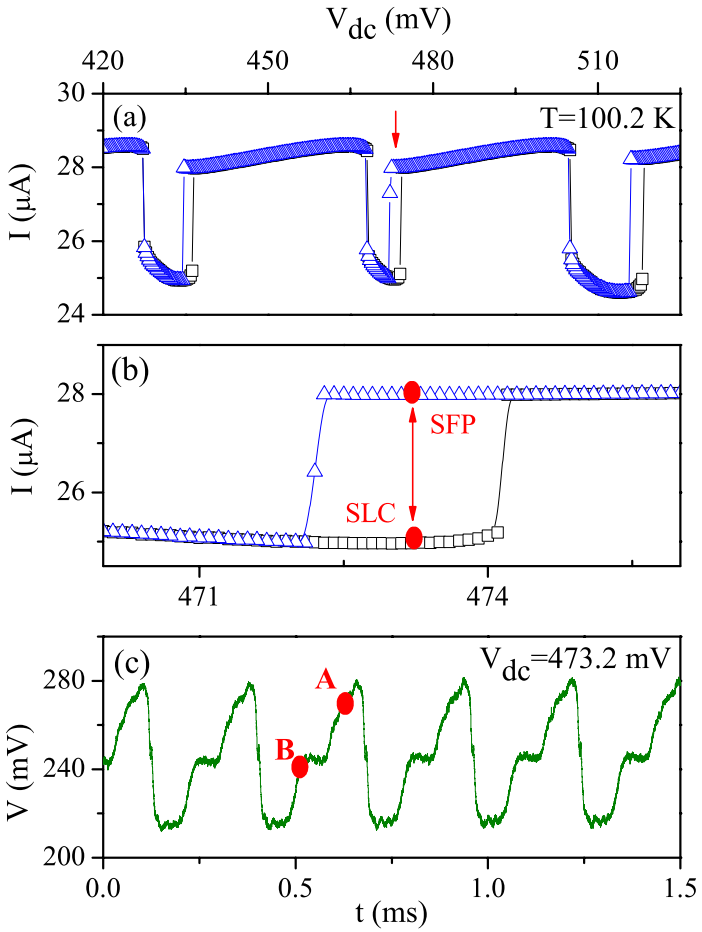

Figure 2. (a) A part of the I–V curve on the first tunneling plateau measured in both sweep-up (open square) and sweep-down (open triangle) directions showing three DVBs; (b) the enlargement of the hysteresis region marked by the arrow in (a) with SLC and SFP states indicated; (c) an SSCO obtained in the SLC state with $V_{dc} = 473.2$ mV. Note that the real-time current trace has been converted to a voltage signal by the Stanford SR570 current preamplifier before being recorded by the Agilent Infiniium 54830B digital oscilloscope, so the vertical axis is a voltage axis.

lower branch an SLC solution. Figure 3(c) shows an SSCO obtained on the lower branch with $V_{dc} = 195.8$ mV, the period of which is around 40 μs.

In order to determine the nature of the bifurcation occurring at the right boundary of the DVB, numerical simulations have been performed to show the dependences of the peak-to-peak current density, J_{p-p}, and the frequency, f, of the calculated SSCO on the applied dc bias, V_{dc}, while V_{dc} increases towards the bifurcation point V_0 (indicated by a vertical arrow in figure 3(b)). The obtained results are shown in figure 4. As V_{dc} approaches V_0, J_{p-p} decreases and f increases. Both J_{p-p} and f obey the same scaling law: $J_{p-p} \sim O(1)$ and $f \sim O(1)$. This is a generic scaling law for the saddle-node bifurcation of cycles [21], i.e. an unstable limit cycle and a stable limit cycle collide at the bifurcation point V_0. Furthermore, it can also be expected that the unstable limit cycle would shrink with decreasing dc bias and eventually engulf the SFP at

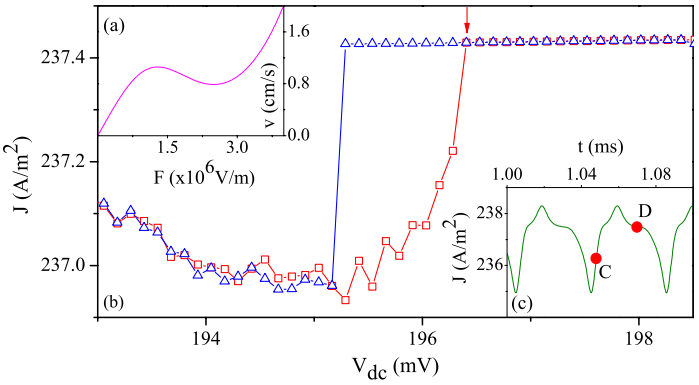

Figure 3. Drift velocity curve used in the simulation (a), the J–V curve calculated in both sweep-up and sweep-down directions (b), and an SSCO calculated in the hysteresis region with $V_{dc} = 195.8\,\text{mV}$ (c).

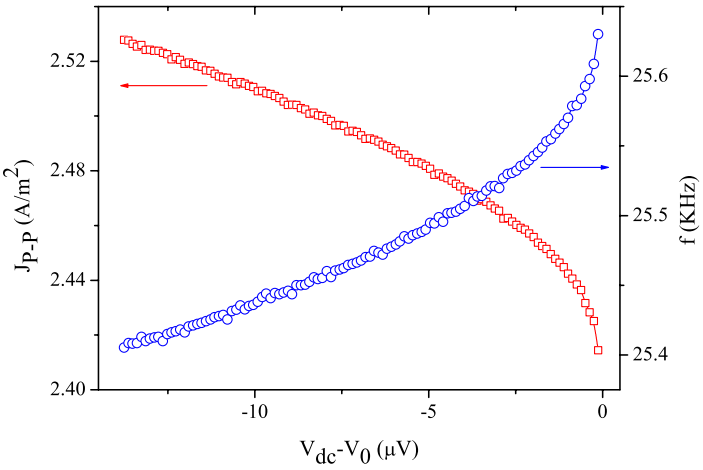

Figure 4. The calculated V_{dc} dependence of J_{p-p} and f in the vicinity of V_0.

the left boundary of the hysteresis, giving rise to a subcritical Hopf bifurcation. Therefore, the bistability disappears via a subcritical Hopf bifurcation and a saddle-node bifurcation of cycles at the left and right boundaries, respectively. This bifurcation scenario is the same as that in [14], but different from that in [6], where supercritical Hopf bifurcation and homoclinic bifurcation were predicted theoretically.

3.2. Pulse-induced transition from SLC to SFP

The transition from SLC to SFP is studied utilizing the phase-dependent pulse generation scheme as shown in figure 1. The SL system with $V_{dc} = 473.2\,\text{mV}$ is initially at the SLC state as marked by a red dot on the lower current branch in figure 2(b), and then a rectangular voltage pulse is applied as a perturbation to the SL system, with the pulse width and height denoted by Δ and h, respectively. The results for two different phase positions A and B, marked by the red dots in figure 2(c), are shown here. Figures 5(a) and (b) show the transition efficiency (η) obtained under different pulse conditions for phases A and B, respectively. η is defined as the

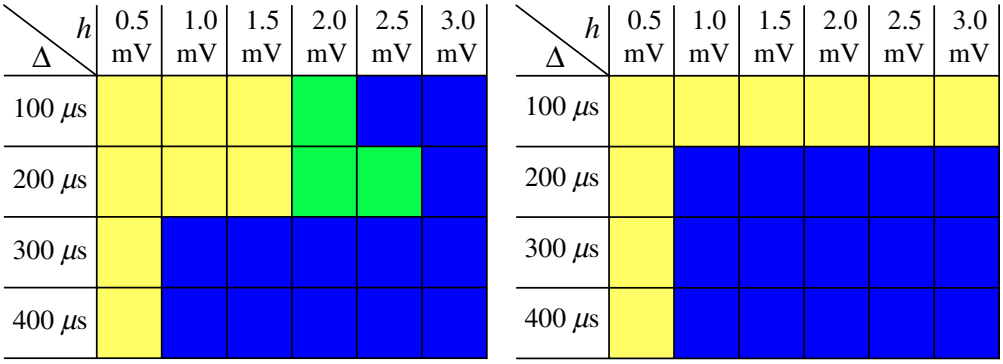

Figure 5. η obtained under different pulse conditions for phase A (a) and phase B (b) in the transition from SLC to SFP.

probability of obtaining a successful transition from SLC to SFP per pulse generation. The blue, yellow and green colored squares (or black, white and gray in gray scale) in figures 5(a) and (b) correspond to $\eta = 1$, $\eta = 0$ and $0 < \eta < 1$, respectively. The different distributions of various colored squares between figures 5(a) and (b) for various values of Δ and h clearly reveal the phase-dependent character of the transition from SLC to SFP. The blue squares appearing in both figures 5(a) and (b), especially for larger values of Δ and h, demonstrate the successful transitions from SLC to SFP induced by the applied voltage pulse. For phase A, the transition from SLC to SFP can be achieved with the minimum Δ of 100 μs, only about one third of SSCO period, τ, while for phase B, the minimum Δ required is 200 μs. In addition, for phase A stochastic transitions are observed (see green colored squares in figure 5(a)). We have also investigated the transition from SLC to SFP with the same pulses of opposite polarity, i.e. $h < 0$, but no successful transitions are observed (data not shown).

SFP and SLC correspond to zero-dimensional and one-dimensional (1D) attractors, respectively, in the phase space. There are attracting basins for SFP and SLC in the phase space. Any phase flow falling into an attractor's basin will be attracted and finally settle down on that attractor. Generally speaking, in steady state of a bistable system the system settles down on one of the two attractors depending on the initial conditions. A dynamic perturbation can drive the system away from the initial attractor to a transient intermediate state. After the perturbation the system will return to a steady state. But depending on the basin of attraction where the transient intermediate state is located, the system can settle down on either its initial attractor or the other attractor. In the latter case, the transition between the bistable states of the system is achieved. Indeed for the bistable SL system studied here, the voltage pulse-induced transitions from SLC to SFP (as shown in figure 5) and the transitions from SFP to SLC (discussed in the next section) are clearly observed. Most interestingly, we note that the SLC is a 1D attractor in the phase space and it consists of an infinite number of phase points. Starting from different phase points the system will evolve to different intermediate states even when the same perturbation is applied. As a result, the transition from SLC to SFP through a transient process is phase-dependent. The difference between figures 5(a) and (b) as discussed above clearly demonstrates this inherent phase dependence. Furthermore, it is possible that the perturbation-induced transient intermediate state is located in the vicinity of the phase boundary of the two attracting basins of SLC and SFP. Under this condition, whether the system will finally evolve

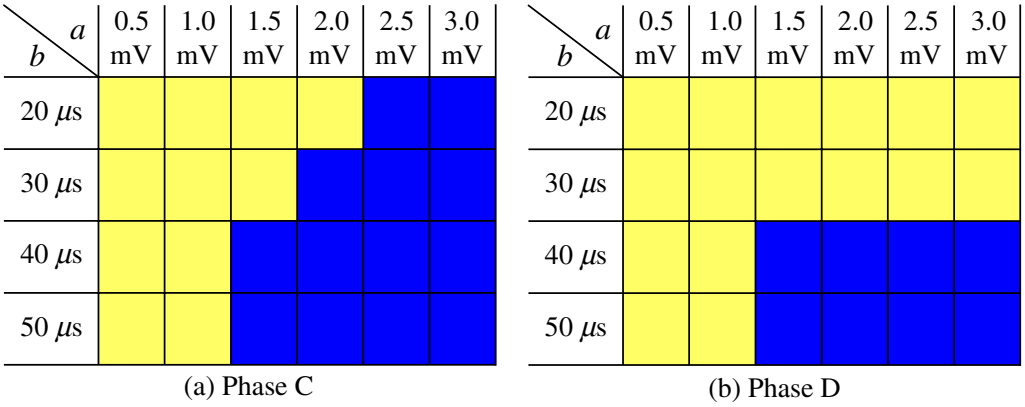

Figure 6. η obtained under different pulse conditions for phase C (a) and phase D (b).

to the new target state is mainly determined by random noises presented in the experiments. This leads to stochastic transitions ($0 < \eta < 1$) as observed in figure 5(a). As for the pulse polarity-dependent features mentioned above, it is believed that they are closely associated with the detailed phase structures of the SL system in the multidimensional phase space. Different relative distribution of SLC and SFP and anisotropic attracting basins of SLC and SFP are possible reasons for this polarity dependence.

To confirm the phase-dependent transition from SLC to SFP, we also performed a numerical simulation using the discrete drift model. The transitions from SLC to SFP at $V_{dc} = 195.8\,\text{mV}$ for two phase positions C and D, as indicated by red dots in figure 3(c), are investigated with a voltage Gaussian pulse defined by: $a^* \exp(-t^2/b^2)$, where a is the pulse height and b specifies the pulse width. Note that using a Gaussian pulse instead of a rectangular pulse in the simulation does not change the essence of the problem.

Figures 6(a) and (b) show the η obtained under different pulse conditions for phase points C and D, respectively. One can see that these numerical results are qualitatively the same as the experimental ones shown in figures 5(a) and (b). Successful transitions from SLC to SFP for phases C and D by applying the Gaussian pulse to the SL system are achieved and the difference between figures 6(a) and (b) confirms the inherent phase dependence of the transition from SLC to SFP. Since noise is negligible in the numerical simulation, stochastic transitions are not observed in figures 6(a) and (b).

3.3. Pulse-induced transition from SFP to SLC

The transition from SFP to SLC is also investigated, but this time the pulse generation is triggered manually instead of phase-dependently. Figure 7 shows the η obtained experimentally under different pulse conditions. Note that the pulse polarity is opposite to that used in SLC to SFP transitions (see figure 5). Blue colored squares in figure 7 clearly demonstrate the successful transitions from SFP to SLC. Since an SFP corresponds to a single phase point in the phase space, no phase dependence exists in the transition from SFP to SLC. This is a striking difference compared to the transition from SLC to SFP. It is also noted that no successful transitions from SFP to SLC are observed when the pulse polarity is changed (data not shown). Besides these, the same minimum absolute value of h in figures 5 and 7 suggests comparable size of the attracting

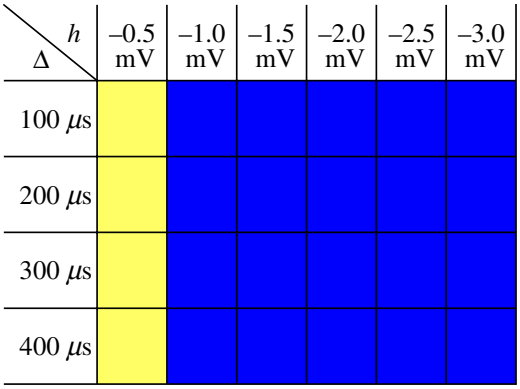

Figure 7. η obtained experimentally under different pulse conditions in the transition from SFP to SLC.

basins of SLC and SFP at $V_{dc} = 473.2$ mV. This is consistent with the fact that the applied dc bias is right in the middle of the hysteresis region, as shown in figure 2(b), since one could expect that the closer to the left (or right) boundary of the bistable region the applied dc bias is, the larger the attracting basin of SLC (or SFP) is.

In the above, we have investigated the bistable transitions between SFP and SLC induced by a voltage pulse. The pulse widths used are of the order of the intrinsic SSCO period. So the perturbation is a fast transient process and the response of the system is dynamic. This is completely different from achieving the transitions between SFP and SLC by controlling the dc voltage sweep (see figures 2(a) and (b)) as in the dc voltage sweep the system reaches a steady state at each applied dc voltage and the response of the system is static.

4. Conclusion

A bistability is observed in each DVB of a weakly-coupled GaAs/AlAs SL, which indicates the coexistence of SLC and SFP states at a given dc bias in the phase space. At the left boundary of the hysteresis, the SFP branch disappears via a subcritical Hopf bifurcation, while at the right boundary, the SLC branch vanishes through a saddle-node bifurcation of cycles. Controllable transitions between these two states through a transient process can be achieved successfully by applying an external voltage pulse as a dynamic perturbation. More importantly, it reveals the phase-dependent feature in the pulse-induced transition from SLC to SFP, which is in agreement with a numerical simulation based on the discrete drift model. In conclusion, the pulse-induced transition scheme as shown in sections 3.2 and 3.3 can be generally applied to any bistable system with bistability between two SFPs, or between SFP and SLC. In order to obtain controllable transitions between bistable states, the minimum requirement of the perturbation is to drive the system to a transient intermediate state located within the attracting basin of the target state. Once this requirement is satisfied, the system will evolve towards the target state after a transient process. But different from the bistable transition from SFP to SFP, or from SFP to SLC, the pulse-induced transition from SLC to SFP exhibits a unique phase-dependent character. This phase dependence is an inherent property in transitions from SLC to SFP through a transient process regardless of the detailed dynamics of the bistable system. As a result, the phase position of the SLC, where a perturbation is applied, is an additional control parameter

for successful transitions from SLC to SFP. Besides these, the pulse polarity dependence and the minimum requirement of the pulse revealed in the pulse-induced transitions between SFP and SLC also provide some information about the attracting basins of SFP and SLC in the phase space.

Acknowledgments

We are grateful to Professor Y P Zeng of the Institute of Semiconductors of CAS for kindly providing the SL samples. We thank the Research Grant Council of HKSAR for financial support via grant 600804.

References

[1] Esaki L and Chang L L 1974 *Phys. Rev. Lett.* **33** 495
[2] Grahn H T, Haug R J, Müller W and Ploog K 1991 *Phys. Rev. Lett.* **67** 1618
[3] Kastrup J, Grahn H T, Ploog K, Prengel F, Wacker A and Schöll E 1994 *Appl. Phys. Lett.* **65** 1808
[4] Prengel F, Wacker A and Schöll E 1994 *Phys. Rev.* B **50** 1705
[5] Kastrup J, Klann R, Grahn H T, Ploog K, Bonilla L L, Galán J, Kindelan M, Moscoso M and Merlin R 1995 *Phys. Rev.* B **52** 13761
[6] Kastrup J, Hey R, Ploog K H, Grahn H T, Bonilla L L, Kindelan M, Moscoso M, Wacker A and Galán J 1997 *Phys. Rev.* B **55** 2476
[7] Sánchez D, Moscoso M, Bonilla L L, Platero G and Aguado R 1999 *Phys. Rev.* B **60** 4489
[8] Amann A, Wacker A and Schöll E 2002 *Physica* B **314** 404
[9] Zhang Y H, Kastrup J, Klann R, Ploog K and Grahn H T 1996 *Phys. Rev. Lett.* **77** 3001
[10] Luo K J, Grahn H T, Ploog K H and Bonilla L L 1998 *Phys. Rev. Lett.* **81** 1290
[11] Amann A, Peters K, Parlitz U, Wacker A and Schöll E 2003 *Phys. Rev. Lett.* **91** 066601
[12] Amann A and Schöll E 2005 *J. Stat. Phys.* **119** 1069
[13] Hizanidis J, Balanov A, Amann A and Schöll E 2006 *Phys. Rev. Lett.* **96** 244104
[14] Luo K J, Teitsworth S W, Kostial H, Grahn H T and Ohtani N 1999 *Appl. Phys. Lett.* **74** 3845
[15] Patra M, Schwarz G and Schöll E 1998 *Phys. Rev.* B **57** 1824
[16] Sun Z Z, He H T, Wang J N, Wang S D and Wang X R 2004 *Phys. Rev.* B **69** 045315
[17] Wang J N, Sun B Q, Wang X R, Wang Y Q, Ge W K and Wang H L 1999 *Appl. Phys. Lett.* **75** 2620
[18] Bonilla L L, Galán J, Cuesta J A, Martínez F C and Molera J M 1994 *Phys. Rev.* B **50** 8644
[19] Bonilla L L 2002 *J. Phys.: Condens. Matter* **14** R341
[20] He H T, Sun Z Z, Wang X R, Wang Y Q, Ge W K and Wang J N 2005 *Solid State Commun.* **136** 572
[21] Strogatz S H 2000 *Nonlinear Dynamics and Chaos* (Boulder, CO: Westview Press) pp 260–5